Scientific Research Publishing

Optics and Photonics Journal, 2023, 13, 178-187
https://www.scirp.org/journal/opj
ISSN Online: 2160-889X
ISSN Print: 2160-8881

Smart Microcavity on the Tip of Multi-Core Optical Fiber for Gas Sensing

Yuqian Zheng, Shengfei Feng

Department of Physics, Capital Normal University, Beijing, China
Email: 342399745@qq.com

How to cite this paper: Zheng, Y.Q. and Feng, S.F. (2023) Smart Microcavity on the Tip of Multi-Core Optical Fiber for Gas Sensing. *Optics and Photonics Journal*, **13**, 178-187.
https://doi.org/10.4236/opj.2023.137016

Received: July 13, 2023
Accepted: July 28, 2023
Published: July 31, 2023

Abstract

We designed and fabricated a smart microcavity sensor with a vertically coupled structure on the end face of a multi-core fiber using two-photon lithography technology. The influence of gap in vertical coupling structure on the resonance characteristics of bonding and anti-bonding modes in the transmission spectrum was studied through simulation and experiments. The results indicate that the bonding and anti-bonding modes generated by the vertical coupling of the two microcavities, as well as the changes in the radius and refractive index of the micro-toroid, and the distance between the microcavities caused by the absorption of vapor during the gas sensing process, exhibit different wavelength shifts for the two resonant modes. Smart microcavity sensors exhibit sensitivity and sensing characteristics.

Keywords

WGM Optical Microcavities, Dual Coupled Microcavity, Bonding and Anti-Bonding Mode, Organic Gas Sensing

1. Introduction

"Lab on fiber" technology is an important branch of fiber optic sensing and micro-nano optics, as well as an important pathway for developing and manufacturing high-performance optoelectronic devices [1] [2]. Furthermore, the two-photon polymerization laser direct writing 3D printing technology makes use of the characteristics of the two-photon absorption process, which has good penetrability to materials and high spatial selectivity [3] [4]. The main advantage of this technology is that it can accurately locate three-dimensional structures and produce high-quality three-dimensional microstructures with high resolution [5] [6]. At present, this technology is becoming an important means of microfabrication, driving the development of manufacturing complex micro nano de-

vices. The use of two-photon lithography technology to prepare and construct micro-nano optical structures on the fiber end face is an effective way to achieve lab on fiber.

On the other hand, optical confinement with nanoscale regions can greatly improve sensitivity and compact optoelectronic devices [7]. The dual coupled microcavity structure with an air gap can limit the evanescent field to the low refractive index region, enhance the overlap range of mode fields and the sensitivity to material perception. This type of slot structure has enormous potential in many applications such as sensing, nonlinear optics, and nanomanipulation [8] [9] [10] [11]. Meanwhile, the optical microcavity based on the whispering-gallery-mode is widely used in sensing because of its small size, low cost and portability [12] [13] [14]. How to further improve the sensing sensitivity of organic vapor micro nano sensing devices based on fiber end coupling is an important research topic in the field of fiber optic sensing. On the one hand, finding device design configurations and sensing mechanisms with better sensing performance is of great theoretical significance. On the other hand, developing new preparation processes for novel sensing configurations in experiments has practical value [15].

In this paper, we report our work on the design, fabrication, and vapor sensing characterization of a smart microcavity with vertical coupling integrated on the end facet of a seven-core optical fiber. By utilizing the dual layer coupled microcavities to support bonding and anti-bonding whispering-gallery-mode, and with different gaps between the dual layer coupled microcavities, the two modes shift towards short and long wavelengths to achieve improved sensing sensitivity.

2. Structure Design and Simulation Analysis

2.1. Microsensor Configuration on the Tip of Fiber

Here, we demonstrate a microcavity sensor on the tip of seven core fiber (see **Figure 1**). The structure is consisting of a pair of vertically stacked micro-toroid (IPL-780 photoresist) separated by a nanoscale gap, and forms a horizontal air-waveguide. The micro-pillars, the micro-prisms, the micro-tapper, and the micro-waveguides form an optical input and output channels. The two micro-pillars are exactly located on the two alternating cores of the seven-core optical fiber, the micro-toroid is held by a pedestal, and the micro-waveguide is supported by connected a micro-ring. The purpose is to avoid significant deformation caused by the suspension of the micro-toroid in the air, and to minimize the degree of deformation of the waveguide caused by surface tension during the development process.

The main parameters of the micro-cavity are as follows. The gap between the micro-toroid and the micro-waveguide is 0.5 μm. The outer radius of the micro-toroid is 18.5 μm, the inner radius is 12 μm, the width is 6.5 μm, respectively. The parameters of the upper and lower micro-toroid are the same. The

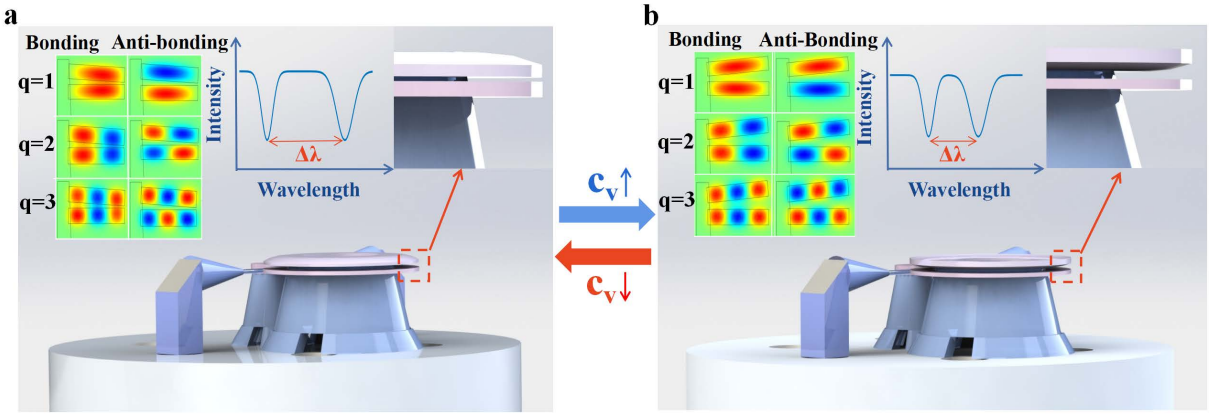

Figure 1. Schematic of the vertically coupled micro-toroid cavity sensor on the end face of seven-core optical fiber. (a) Schematic of the structure before entering the steam. (b) Schematic of the structure after leaving the steam. In the inset, the left image shows the optical profile distribution of the micro-toroid cavity, the middle is a diagram of the resonance mode spectrum, and the right image is an enlarged view of the details of the micro-toroid cavity.

thickness of the lower micro-toroid is 1 μm, the thickness of the upper micro-cavity is 1.5 μm. In addition, the radius of the micro-ring supporting the waveguide is 3.5 μm. The index of the micro-cavity is 1.52.

Part of the laser in the waveguide is coupled into the micro-toroid cavity, with another part of the optical coupling entering the micro-ring cavity. The whispering-gallery-mode (WGM) microcavity excited resonance peak. The bandwidth with a relatively small radius is larger, and with the large radius is smaller. The transmission spectrum shows that the resonance peak with larger bandwidth is superimposed with the narrower resonance peak. The narrow resonance peak has higher Q value and greater sensitivity.

2.2. Numerical Simulation Analysis

In order to investigate the mode profile distribution and optical characteristics of vertically coupled micro-toroid cavities, we used COMSOL to simulate the dynamic changes of microcavities during the sensing process. The cross-sectional view of the model is shown in the inset in the upper right corner of **Figure 1**.

According to the simulation results, when the gap between two microcavities is small enough for vertical optical coupling. As a result of the coupling, the transverse mode profile splits into bonding and anti-bonding modes combination. The inset in **Figure 1** shows the mode profile of the first-order (q = 1), the second-order (q = 2) and the third-order (q = 3), respectively. Bonding modes attract and anti-bonding modes repulsive. In the process of vapor sensing, as the vapor concentration increases, the vertically coupled micro-toroid approach each other. The micro-toroid is far away from each other while the concentration decreases. The resonance peaks are far away from each other and close to each other in the spectrum. In the transmission spectrum, the resonance peaks show that attractive and repulsive, respectively. **Figure 1(a)** to **Figure 1(b)** show the forward process of the device from air to vapor during the sensing process, conversely.

3. Experiments

3.1. Confirmation Experiments

In order to realize hetero-structures in a single manufacturing step, it is necessary to achieve control over material properties. Therefore, we investigated the effect of laser direct writing intensity on photoresist materials. We utilize the flexibility of 3D laser lithography to change the local exposure dose during the writing process. This method enables us to realize materials with substantially different properties in one manufacturing step from a single photoresist formulation [16] [17].

Before preparing the sensor component, a confirmation experiment was conducted. On the tip of the optical fiber, the micro-cuboids are manufactured as bases, and the suspended micro-strips are embedded on the side of the micro-cuboids. Two different laser intensities are used for writing micro-stripes directly (yellow represents the weak laser intensity, and blue represents the strong laser intensity). The top view of the designed structure is shown in **Figure 2(a)** and **Figure 2(b)**. The corresponding samples prepared are shown in **Figure 2(c)** and **Figure 2(d)**. From the results under the microscope, it can be seen that the micro-strips in **Figure 2(c)** are bent inward, while the microstrips in **Figure 2(d)** are bent outward. The middle group is not bent, and both groups have a greater degree of bending than the right group (from top to bottom as a group). Because the magnitude of material shrinkage and hardening effects largely depends on the crosslinking density of the photoresist [18]. The photoresist will shrink to a certain extent due to the polymerization effect after exposure [19] [20]. The photoresist with large crosslinking degree will shrink, while the

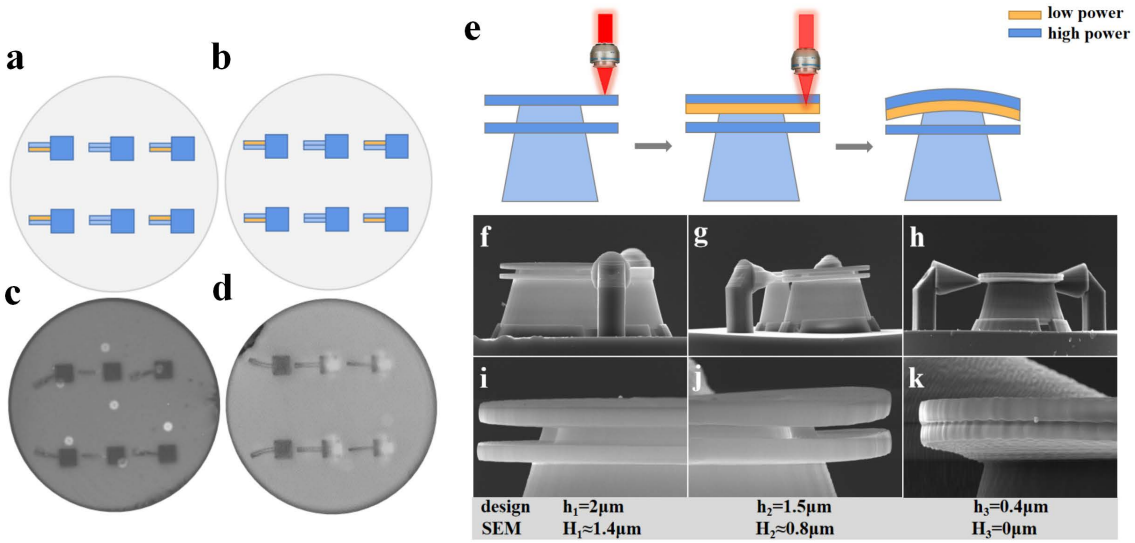

Figure 2. Design structure and microscope image of reference experiment and vertically coupled micro-toroid cavity sensor. (a), (b) Schematic of the reference experimental structure. (c), (d) Microscopic view of experimental results in (a) and (b). (e) The preparation process of vertically coupled micro-toroid cavity. (f)-(h) SEM of vertically coupled microcavity with different *h* prepared after sensing. (i)-(k) The enlarged images of the corresponding details.

photoresist with small crosslinking degree will shrink greatly. As a result, the crosslinking density of the parts of written by strong laser is higher than the parts of weak laser. The polymer network formed by weak light is relatively loose, and the inner side (lower crosslinking density) shows stronger shrinkage than the outer side (higher crosslinking density), which leads to a significant inward bending.

Figure 2(e) shows the preparation process of microcavity using laser control. When preparing two vertically stacked micro-toroid cavities, the upper surface of the upper micro-toroid is directly written with strong laser, and the lower surface with weak laser. The lower micro-toroid only use the strong laser for direct writing. The outer edge of the upper micro-toroid of the prepared micro sensing device will have a downward trend (when the samples are available).

Figure 2(f) to **Figure 2(h)** are the electron microscope images of the micro-sensor sample after isopropanol (ISO) vapor solution sensing experiment. The gap (h) of the vertically stacked micro-toroid is 2 μm, 1.5 μm, 0.4 μm, respectively. **Figure 2(i)** to **Figure 2(k)** are the corresponding detailed drawings. It can be seen that after sensing test, the outer edge of the upper micro-toroid tends to tilt upwards. Because the degree of photo-crosslinking between the upper and lower surfaces of the upper micro-toroid cavity is different, and the density of the polymer network on the lower surface is relatively loose, which can adsorb more organic molecules than the upper surface. Therefore, as the concentration of organic solution increases, the outer edge of the upper micro-toroid cavity will have a tendency to tilt upwards and gradually move away from the lower micro-toroid cavity.

In the SEM images, the actual parameters used for micro-toroid gap are approximately 0.6 μm smaller than the designed parameters measured after gas sensing. This is probable as a result of the slight change of the material caused by the environment when shooting the scanning electron microscope in vacuum, plus the fact that the structure will not completely recover to its original state after the gas sensing.

3.2. Sensing Characteristics

We characterize vapor sensing characterizations of smart cavity in the ISO vapor solution.

Due to the red-shift of the resonance peak caused by the material swelling, and the mode splitting caused by the coupling of two micro-toroid cavities, for the convenience of research, we align one of the resonance modes in the spectrum and observe the relative changes of other resonance modes.

Figure 3(a) and **Figure 3(b)** are the transmission spectrum of ISO vapor sensing. **Figure 3(a)** is the sample h = 2 μm in ISO organic vapor with concentrations ranging from 10% to 50%. After aligning the first resonance peak on the spectrum near 1526 nm, it is found that the relative position of the resonance peak at other concentrations and at 10% concentration are basically unchanged,

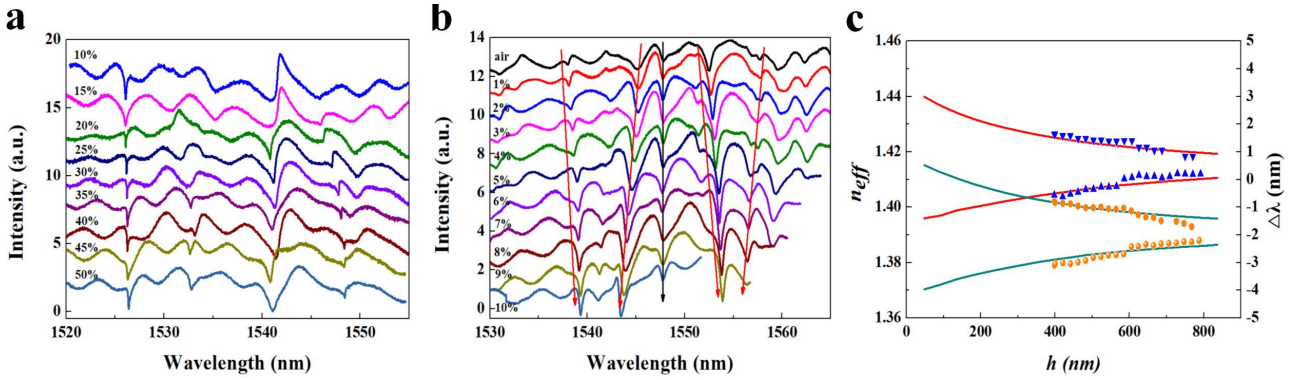

Figure 3. Sensing characteristics of vertically coupled microcavities. (a) Spectra after aligned to a resonance mode of the sample h = 2 μm located in vapors of ISO solutions with varying concentrations from 10% to 50% in steps of 5%. (b) Spectra after aligned to a resonance mode of the sample h = 0.4 μm located in vapors of ISO solutions with varying concentrations from 0% to 10% in steps of 1%. (c) The variation curve of the vertical coupling microcavity spacing with the effective refractive index of the microcavity and the resonance peak drift, the triangle and the point are the experimental results, and the solid line is the exponential fitting results.

indicating that only the red-shift of the resonance mode caused by swelling occurs at this interval h. **Figure 3(b)** is the sample h = 0.4 μm in ISO organic vapor with concentrations ranging from 1% to 10%. After aligning the resonance peak at about 1548 nm in the transmission spectrum, we found that there was a pair of obvious resonance modes on the left and right sides of the reference resonance peak (black arrow line). With the increase of organic vapor concentration, the pair of resonance modes gradually approached to each other. When the h is small enough, the vertical coupling of the two microcavities cause mode splitting, forming bonding and anti-bonding modes.

During the process of placing the sample in air and ISO vapor solution, as the concentration increases, more and more organic molecules are adsorbed on the surface of the upper microcavity, resulting in swelling effect. The edge of the cavity tends to expand and compress upwards. In this process, the optical field of bonding mode moves inward, so the effective radius of the micro-toroid cavity becomes smaller, and the resonant mode is shifting blue. The optical field of the anti-bonding mode moves towards the outer edge of the toroid, the effective radius of the micro-toroid cavity becomes larger, and the resonance mode is shifting red.

In summary, a pair of bonding and anti-bonding modes generated by mode splitting which show a red-shift and a blue-shift as the organic vapor concentration increases. The resonance peaks of the two modes gradually approach in the spectrum. Moreover, the variation of first-order, second-order, and third-order modes are different, the relative wavelength and sensitivity of this variable is also different.

The two pairs of bonding and anti-bonding modes shown in **Figure 3(b)** are located within a free spectral range (approximately 16 nm), which can be considered as excitation of first-order and second-order modes. The movement of the optical field distribution will cause the change of the effective radius of the mi-

cro-toroid cavity, and the effective refractive index will also be different.

We simulated the optical field distribution at different h, obtained the effective refractive index *neff* corresponding to the first and second order modes of bonding and anti-bonding modes, and obtained the relationship of h – *neff* as shown in **Figure 3(c)**. From top to bottom, the red curve represents the bonding and anti-bonding modes of the first order, while the teal curve represents the second order. The scatter points on the graph are taken from the sample h = 0.4 μm, the relative wavelengths of a pair of bonding and anti-bonding modes.

When the gap between the two micro-toroid cavities becomes larger and larger, so that the optical fields of the two cavities do not affect and will not be coupled, the mode splitting disappears, and the bonding and anti-bonding modes will eventually merge into a resonance peaks. The simulation and experimental results are consistent.

3.3. Sensing Characteristics

Figure 4 shows the dynamic process of a vertically coupled smart microcavity gas sensor in organic vapor concentration.

We were set the sample h = 0.4 μm place in a vapor environment of a saturated solution of ISO. Record the transmission spectra of the sample for all cycles within the scanning range of 1520 - 1570 nm wavelength, within 0 - 200 seconds of entering and 200 - 400 seconds of leaving the vapor environment. take the relative wavelength differences of all first-order bonding and anti-bonding modes Δ λ, record two cycles. During the sensing process, the number of organic molecules absorbed by the material increases as the concentration increases, and the bonding and anti-bonding modes approach to each other, while the opposite is true. The relatively small change in wavelength difference after the second addition of steam perhaps it is because after leaving the vapor environment, there are still organic molecules left in the cavity, and the sample has not recovered, so the experiment for the second cycle begins, which affects

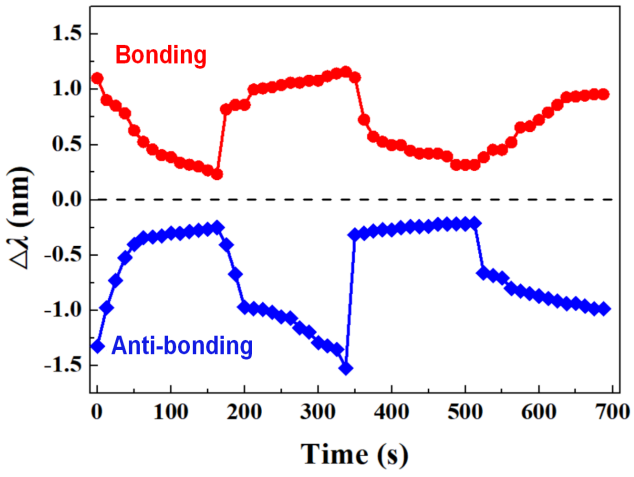

Figure 4. The relative drift of bonding and anti-bonding modes of microcavity sensors entering and leaving ISO vapor over time (scatter points are experimental data).

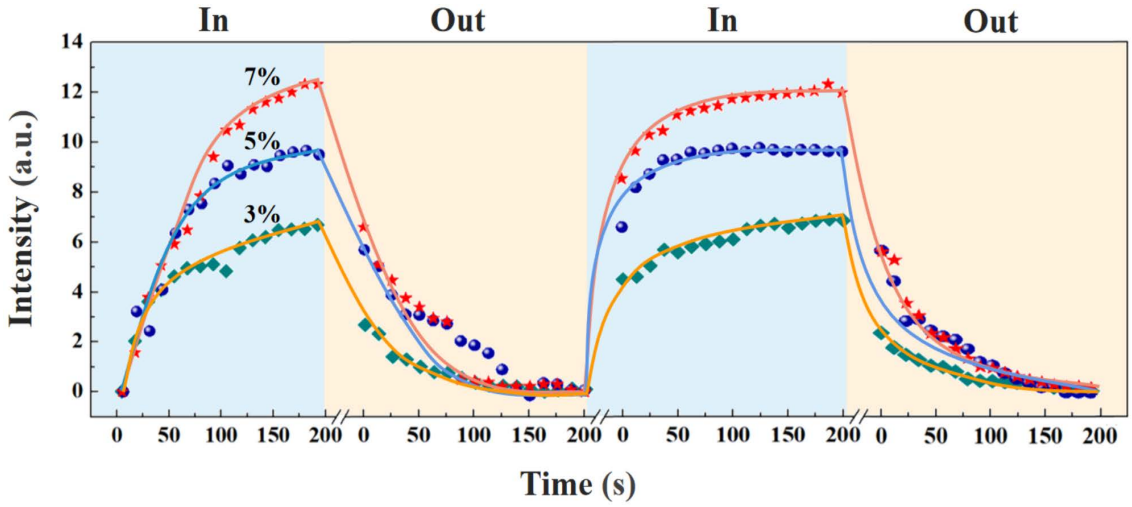

Figure 5. Two cycle tests on the reversibility of vertically coupled microcavity sensors in steam with different ISO concentrations. Exponential fit between solid lines and experimental data (scatter points).

the variation of the gap of microcavity in the second cycle.

In order to characterize the time response of the microsensor, the sample was placed in ISO organic vapor for 200 seconds, and the spectra of each 1520 - 1570 nm wavelength scanning range were recorded. The sample was then taken out and placed in air for 200 seconds, and all spectra within the 1520 - 1570 nm wavelength scanning range were also recorded. This process undergoes two cycles. We tested the concentrations of 3%, 5%, and 7%, respectively.

As shown in **Figure 5**, the trend curves are best fitted according to the Langmuir isotherm after data processing, where the scattered points correspond to the data results extracted from the experiment. The fitting curve is consistent with the experimental results. The rise time response rates were 6.8 nm/s, 9.7 nm/s, 12.3 nm/s, and the fall time response rates were 3.9 nm/s, 5.8 nm/s, and 6.7 nm/s, respectively.

4. Conclusion

In summary, we propose and demonstrate use of two-photon lithography technology to manufacture smart microcavity sensors on the end face of seven-core fiber. We simulated the optical profile distribution and the mode analysis of vertically coupled microcavities with different gaps, especially the bonding and anti-bonding modes. We show the experimental results of the dynamic changes of the smart microcavity and characterization of sensing performance in isopropanol vapor during sensing, which is helpful for analyzing sensing process and improving sensing sensitivity.

Acknowledgements

This work was supported by the National Natural Science Foundation of China, No. 61735002. We also acknowledge the Lab for Three-Dimensional Lithography of the Department of Physics, Capital Normal University.

Conflicts of Interest

The authors declare no conflicts of interest regarding the publication of this paper.

References

[1] Xiong, Y. and Xu, F. (2020) Multifunctional Integration on Optical Fiber Tips: Challenges and Opportunities. *Advanced Photonics*, **2**, No. 6. https://doi.org/10.1117/1.AP.2.6.064001

[2] Vaiano, P., Carotenuto, B., Pisco, M., *et al.* (2016) Lab on Fiber Technology for Biological Sensing Applications. *Laser & Photonics Reviews*, **10**, 858. https://doi.org/10.1002/lpor.201670066

[3] Qu, J., Kadic, M., Naber, A., *et al.* (2017) Micro-Structured Two-Component 3D Metamaterials with Negative Thermal-Expansion Coefficient from Positive Constituents. *Scientific Reports*, **7**, Article Number: 40643. https://doi.org/10.1038/srep40643

[4] Chen, Y.G., Tang, S.K., Zhang, Y.Q., *et al.* (2010) *Zhihengliuella salsuginis* sp. nov. a Moderately Halophilic Actinobacterium from a Subterranean Brine. *International Journal of Systematic & Evolutionary Microbiology*, **14**, 397-402. https://doi.org/10.1007/s00792-010-0317-4

[5] Principe, M., Consales, M., Micco, A., *et al.* (2017) Optical Fiber Meta-Tips. *Light: Science & Applications*, **6**, e16226. https://doi.org/10.1038/lsa.2016.226

[6] Hahn, V., Kalt, S., Sridharan, G.M., *et al.* (2018) Polarizing Beam Splitter Integrated onto an Optical Fiber Facet. *Optics Express*, **26**, 33148-33157. https://doi.org/10.1364/OE.26.033148

[7] Xu, Q., Almeida, V.R., Panepucci, R.R., *et al.* (2004) Experimental Demonstration of Guiding and Confining Light in Nanometer-Size Low-Refractive-Index Material. *Optics Letters*, **29**, 1626-1628. https://doi.org/10.1364/OL.29.001626

[8] Wiederhecker, G.S., Chen, L., Gondarenko, A., *et al.* (2009) Controlling Photonic Structures Using Optical Forces. *Nature*, **462**, 633-636. https://doi.org/10.1038/nature08584

[9] Lee, S., Eom, S.C., Chang, J.S., *et al.* (2010) Label-Free Optical Biosensing Using a Horizontal Air-Slot SiNx Microdisk Resonator. *Optics Express*, **18**, 20638-20644. https://doi.org/10.1364/OE.18.020638

[10] Zheng, Y., Fang, Z., Liu, S., *et al.* (2019) High-Q Exterior Whispering-Gallery Modes in a Double-Layer Crystalline Microdisk Resonator. *Physical Review Letters*, **122**, Article ID: 253902. https://doi.org/10.1103/PhysRevLett.122.253902

[11] Xue, X., Zheng, X. and Zhou, B. (2019) Super-Efficient Temporal Solitons in Mutually Coupled Optical Cavities. *Nature Photonics*, **13**, 616-622. https://doi.org/10.1038/s41566-019-0436-0

[12] Foreman, M.R., Swaim, J.D. and Vollmer, F. (2015) Whispering Gallery Mode Sensors. *Adv Opt Photonics*, **7**, 168-240. https://doi.org/10.1364/AOP.7.000168

[13] Ilchenko, V.S., Gorodetsky, M.L., Yao, X.S., *et al.* (2000) Microtorus: A High Finesse Microcavity with Whispering-Gallery Modes. *Optics Letters*, **26**, 256-258. https://doi.org/10.1364/OL.26.000256

[14] Armani, D.K., Kippenberg, T.J., Spillane, S.M., *et al.* (2003) Ultra-High-Q Toroid Microcavity on a Chip. *Nature*, **421**, 925-928. https://doi.org/10.1038/nature01371

[15] Zhan, Y., Liu, Q., Feng, S., *et al.* (2020) Photonic Molecules Stacked on Multicore

Optical Fiber for Vapor Sensing. *Applied Physics Letters*, **117**, Article ID: 171107. https://doi.org/10.1063/5.0025261

[16] Hippler, M., Blasco, E., Qu, J., *et al*. (2019) Controlling the Shape of 3D Microstructures by Temperature and Light. *Nature Communications*, **10**, 232. https://doi.org/10.1038/s41467-018-08175-w

[17] Ovsianikov, A., Ostendorf, A. and Chichkov, B.N. (2007) Three-Dimensional Photofabrication with Femtosecond Lasers for Applications in Photonics and Biomedicine. *Applied Surface Science*, **253**, 6599-6602. https://doi.org/10.1016/j.apsusc.2007.01.058

[18] Maruo, S., Nakamura, O. and Kawata, S. (1997) Three-Dimensional Microfabrication with Two-Photon Absorbed Photopolymerization. *Optics Letters*, **22**, 132-134. https://doi.org/10.1364/OL.22.000132

[19] Lafratta, C.N., Fourkas, J.T., Baldacchini, T., *et al*. (2007) Multiphoton Fabrication. *ChemInform*, **38**, No. 45. https://doi.org/10.1002/chin.200745266

[20] Mehrabani, S., Kwong, P., Gupta, M., *et al*. (2013) Hybrid Microcavity Humidity Sensor. *Applied Physics Letters*, **102**, Article ID: 241101. https://doi.org/10.1063/1.4811265